Spallation Neutron Production by 0.8, 1.2, and 1.6 GeV Protons on Pb Targets

X. Ledoux,[1] F. Borne,[1] A. Boudard,[3] F. Brochard,[2] S. Crespin,[1] D. Drake,[1] J. C. Duchazeaubeneix,[2] D. Durand,[6] J. M. Durand,[2] J. Fréhaut,[1] F. Hanappe,[7] L. Kowalski,[2] C. Lebrun,[6] F. R. Lecolley,[6] J. F. Lecolley,[6] F. Lefebvres,[6] R. Legrain,[3] S. Leray,[2,3] M. Louvel,[6] E. Martinez,[1] S. I. Meigo,[2] S. Ménard,[5] G. Milleret,[2] Y. Patin,[1] E. Petibon,[1] F. Plouin,[2] P. Pras,[1] L. Stuttge,[8] Y. Terrien,[3] J. Thun,[2,4] M. Uematsu,[2] C. Varignon,[6] D. M. Whittal,[2] and W. Wlazło[2]

[1]*DPTA/SPN, Commissariat à l'Energie Atomique, F-91680 Bruyères-le-Châtel, France*

[2]*Laboratoire National SATURNE, F-91191 Gif-sur-Yvette, France*

[3]*DAPNIA/SPhN, Commissariat à l'Energie Atomique, F-91191 Gif-sur-Yvette, France*

[4]*Uppsala University, S-75121 Uppsala, Sweden*

[5]*Institut de Physique Nucléaire, F-91406 Orsay, France*

[6]*LPC, ISMRa et Université de Caen, CNRS/IN2P3, 6 Boulevard du Marchal Juin, F-14050 Caen CEDEX, France*

[7]*Interactions Ion-Matière, CP 229, Université Libre de Bruxelles, Belgium*

[8]*IReS, Strasbourg, France*

(Received 19 October 1998)

Spallation neutron production in proton induced reactions on Pb targets at 0.8, 1.2, and 1.6 GeV has been measured at the SATURNE accelerator. Double-differential cross sections were obtained over a broad angular range from which averaged neutron multiplicities per reaction were inferred for energies above 2 MeV. The results are compared with calculations performed with a high energy transport code including two different intranuclear cascade (INC) models: it is shown that the Cugnon INC model gives a better agreement with the data than the Bertini one, mainly because of improved nucleon-nucleon cross sections and Pauli blocking treatment. [S0031-9007(99)09196-6]

PACS numbers: 25.40.Sc, 24.10.Lx, 29.25.Dz

Spallation reactions can be used to produce high neutron fluxes by bombarding a thick heavy target with a high intensity intermediate energy proton beam. Interest in spallation reactions has recently been renewed because of the importance of intense neutron sources for various applications, such as spallation neutron sources for condensed matter and material physics [1–3], tritium production [4,5], accelerator-driven subcritical reactors for nuclear waste transmutation [6,7], or energy production [8]. Numerical calculation codes are available to design spallation sources. However, physics models used in these codes to describe elementary nuclear reactions above 20 MeV still suffer from large uncertainties. For instance, in [9], model predictions concerning neutron production double-differential cross sections were found to show big discrepancies between different codes. It was concluded that additional data were necessary, especially above 0.8 GeV, in order to improve and validate the models. Furthermore, neutron energy and angular distributions data are important for a correct simulation of the propagation of particles inside a spallation target and the geometrical distribution of the outgoing neutron flux.

An extensive program has been conducted at the Laboratoire National Saturne to measure energy and angular distributions of neutrons produced by protons and deuterons with energies from 0.8 to 1.6 GeV on various thin and thick targets. In this Letter, we report on the measurement of double-differential cross sections obtained, at angles varying from 0° to 160°, with 0.8, 1.2, and 1.6 GeV proton beams on a 2-cm-thick Pb target. Neutron energy spectra were measured by two complementary experimental techniques, described in detail in [10,11], in a new experimental area [12].

Low energy neutrons ($E_n \leq 400$ MeV) were measured by time of flight between the incident proton, tagged by a plastic scintillator, and a neutron sensitive NE213 liquid scintillator [10]. Up to ten angles could be explored simultaneously using several neutron detectors. Six of them (cells of the multidetector DEMON [13]) were used between 4 and 400 MeV. The other four (called DENSE) allowed energy measurements with a reasonable error from 2 to 14 MeV. A pulse shape analysis was used for neutron-gamma discrimination. The energy resolution associated to this time-of-flight measurement is less than 10% for energies varying from 2 to 400 MeV.

To determine the neutron detector efficiency over the whole energy range, three experiments have been performed: from 2 to 16 MeV at the Bruyères-le-Châtel neutron facility [10], for $30 \leq E \leq 100$ MeV at the Uppsala cyclotron [14], and above 150 MeV with calibrated quasimonoenergetic neutron beams obtained by d + Be breakup reactions at Saturne [10]. Systematic errors in the time-of-flight method come mainly from the subtraction of chance coincidences, gamma rejection, and efficiency determination. They are of the order of 10% except at high energies where the uncertainty on the d + Be cross section makes it poorer but always less than 15%.

High energy measurements ($E_n \geq 200$ MeV) were done using (n, p) scattering on a liquid hydrogen converter and reconstruction of the proton trajectory in a rotating magnetic spectrometer [11]. Absolute calibration

 0031-9007/99/82(22)/4412(4)$15.00

of the beam was obtained by measuring the activation of a carbon sample. The response function of the spectrometer, normalized through (n, p) elastic scattering cross section [15], has been measured using the Saturne quasimonoenergetic neutron beams. It is then used to unfold the measured proton spectra from the inelastic contribution to obtain the incident neutron distributions as described in [11]. Systematic errors in this method arise mainly from the beam calibration and the unfolding procedure: they are less than 15% at 800 and 1200 MeV but can reach 25% at 1600 MeV because of the increasing inelastic contribution.

With both detection systems, a 2-cm-thick lead target had to be used in order to keep a significant counting rate. Error bars on the results presented here take into account only statistical uncertainties except at the very low energies where the increase of uncertainty associated with the proximity of the detection threshold is added. Figure 1 presents 0° momentum spectra obtained at 800 MeV, with the spectrometer, for two different target thicknesses, 2 cm and 1.2 mm, compared with previous data (on a 1 mm target) from Bonner *et al.* [16]. The spectra are composed of several components. The peak close to the beam momentum corresponds to quasielastic (actually charge exchange) *NN* collisions inside the target nucleus. The bump around 1100 MeV/c is associated with pion emission through excitation of the Δ_{33} (1232 MeV) resonance in inelastic *NN* collisions. Neutrons detected at lower momenta arise from processes involving several *NN* collisions. The main difference between the spectra observed when using a thicker target concerns the quasielastic peak: due to the energy lost by the projectile in the target, the peak becomes smaller and wider and its center is shifted towards lower energy. A similar trend is observed for the Δ resonance. Very good agreement is found with the result from [16] when using the similar thickness target.

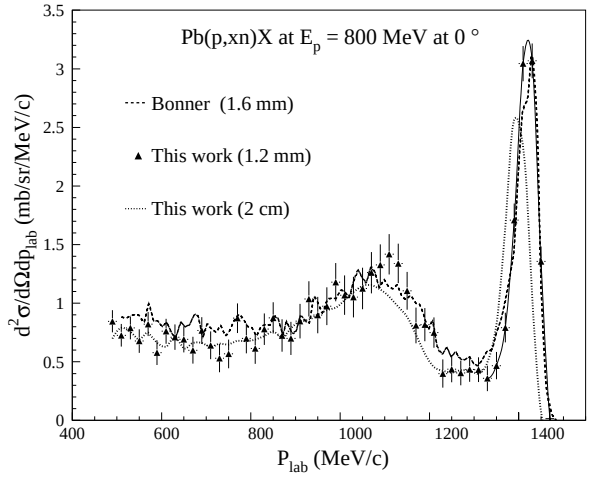

FIG. 1. Neutron production double-differential cross section measured at 0° by the spectrometer technique on two different thickness Pb targets at 800 MeV compared with the data from [16].

Figure 2 displays energy-angle double-differential cross sections measured on the 2-cm-thick lead target at 800 MeV incident protons at 25°, 55°, 130°, and 160° with time of flight and spectrometer. The results obtained at 145° with the DENSE detectors have been extrapolated at 130° and 160° assuming that the neutrons are evaporated ones and therefore isotropically emitted. It has to be stressed that our two experimental techniques are totally independent and agree within 10% in the 200–400 MeV range where they overlap. A very good agreement is observed between this work and previous data obtained by Amian *et al.* [17] with a conventional time-of-flight technique (full lines) at very close angles (30°, 60°, 120°, and 160°) and by Nakamoto *et al.* [18], not shown here. At these angles, the quasielastic and Δ resonance peaks are no longer visible. The low energy neutrons measured with the time-of-flight technique mostly come from evaporation of the excited target nucleus after the intranuclear cascade (INC) stage.

Figure 3 presents neutron cross-section distributions in Pb$(p, xn)X$ reactions at 1200 and 1600 MeV incident energy, respectively. The results obtained by time of flight, with DEMON and DENSE detectors, and with the spectrometer are plotted. Only two DENSE detectors have been used at 1200 MeV (at 25° and 145°). It can be seen that the quasielastic and inelastic contributions disappear above 25°. Between 25° and 85° the spectrometer gives access to the tail of the distribution and actually cross-section measurements over 5 orders of magnitude have been realized. The histograms are Monte Carlo calculations, taking into account the actual geometry and composition of the target, performed with the TIERCE [19] code system developed at Bruyères-le-Châtel. In order

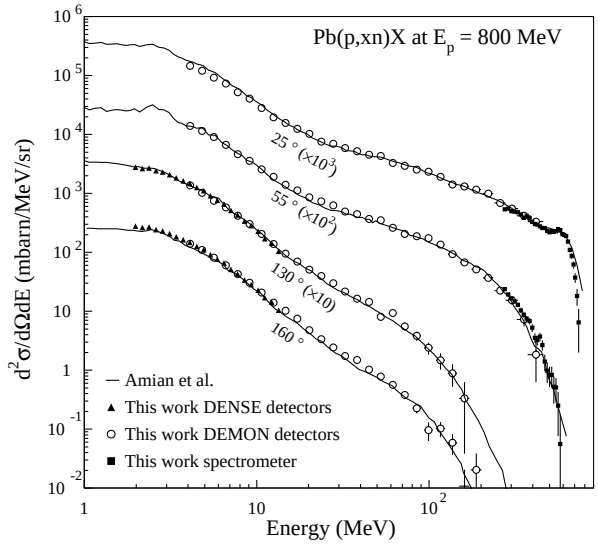

FIG. 2. Neutron production double-differential cross sections measured at 800 MeV on a 2-cm-thick Pb target by time of flight, with DEMON (empty circles) and DENSE (filled triangles) detectors, and the spectrometer (filled squares). The line represents the results obtained by Amian *et al.* [17] at close angles: 30°, 60°, 120°, and 160°.

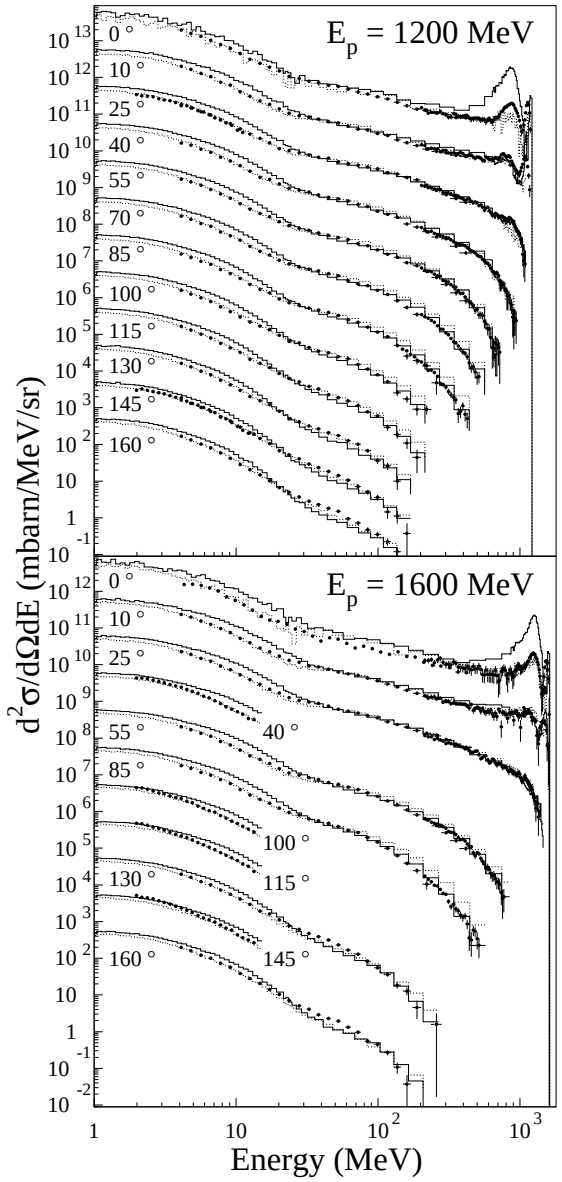

FIG. 3. Neutron production double-differential cross sections measured in proton induced reactions on a 2-cm-thick Pb target at 1200 and 1600 MeV. Each successive curve, from 160°, is scaled by a factor of 10 with decreasing angle. The histograms represent TIERCE calculations [19] using the Bertini [20] (full line) or the Cugnon [21] (dotted line) cascade model followed by the same evaporation model.

to obtain enough statistics, the emission angle is taken as $\pm 2.5°$, which is much larger than the experimental aperture ($\pm 0.43°$ for spectrometer and between $\pm 0.71°$ and $\pm 0.81°$ for time of flight).

TIERCE is essentially composed of a high energy transport code (based on the HETC code from [22]), which generates cross sections through physics models and transports particles above 20 MeV, and MCNP [23] which utilizes evaluated cross-section data to transport neutrons below 20 MeV. Within HETC two different intranuclear cascade codes followed by the same evaporation model [24] have been used: the Bertini [20] (full line) and Cugnon [21,25] (dotted line) models. At 0°, the Bertini cascade predicts a huge peak, which is not experimentally observed, in the region corresponding to the Δ resonance excitation. This problem is known to be due to a too-forward-peaked angular distribution of $NN \rightarrow N\Delta$ reaction in the Bertini INC code. The more realistic parametrization of this angular distribution [26], introduced in the code from Cugnon *et al.* [21] results in the removal of this pathologic behavior as can be seen in Fig. 3. At high energy, both models are in quite good accordance with the data between 10° and 85° but the Bertini code underpredicts the backward angles. Whatever the angle, calculations with the Bertini cascade overestimates the production cross sections below 20 MeV while the Cugnon model generally leads to a much better agreement. This could be explained by the larger excitation energy after the INC phase found in the Bertini rather than in the Cugnon calculation.

The measured and predicted neutron multiplicity, M_n, and kinetic energy carried out by neutrons, $E \times M_n$, per primary reaction averaged, are presented in Tables I and II. To obtain the experimental values, data have been integrated over 4π, by interpolating between the measured angles, then divided by the reaction cross section from TIERCE (which agrees with [27]). Three energy ranges have been considered: 0–2 MeV for model predictions only, 2–20 MeV in which data from DENSE detectors have been extrapolated to DEMON angles between 2 and 4 MeV, and 20-MeV-beam energy. Neutrons in the last bin are cascade neutrons while, below 20 MeV, they come mostly from evaporation. Uncertainties take into account statistical uncertainties plus those associated with the extrapolation procedures. The effect of the 2-cm target thickness has been investigated and found to be negligible in the 2–20 MeV range and less than 10% for the high energy range.

The Bertini calculation largely overpredicts the number of emitted neutrons in the 2–20 MeV range while Cugnon gives rather good agreement, confirming the tendency observed in Fig. 3. Cascade neutron multiplicities

TABLE I. Per primary reaction averaged neutron multiplicities obtained by integration of the double-differential cross sections and compared with calculations using Cugnon or Bertini INC model for a 2-cm Pb target.

Energy	M_n^{exp}	M_n^{Cugn}	M_n^{Bert}
	$E = 800$ MeV, $\sigma_R = 1723$ mb		
0–2 MeV		4.9	6.1
2–20 MeV	6.5 ± 1.0	6.9	9.5
20–E_{beam}	1.9 ± 0.2	2.2	1.8
	$E = 1200$ MeV, $\sigma_R = 1719$ mb		
0–2 MeV		5.8	6.9
2–20 MeV	8.3 ± 1.0	8.9	12.4
20–E_{beam}	2.7 ± 0.3	2.8	2.4
	$E = 1600$ MeV, $\sigma_R = 1717$ mb		
0–2 MeV		6.0	7.4
2–20 MeV	10.1 ± 1.4	9.9	14.7
20–E_{beam}	3.4 ± 0.3	3.1	3.1

TABLE II. Same as Table I but for per primary reaction averaged kinetic energy carried out by the emitted neutrons.

Energy	$E \times M_n^{\mathrm{exp}}$	$E \times M_n^{\mathrm{Cugn}}$	$E \times M_n^{\mathrm{Bert}}$
	$E = 800$ MeV, $\sigma_R = 1723$ mb		
0–2 MeV		5.0	6.0
2–20 MeV	38.0 ± 4.0	42.0	55.0
20–E_{beam}	200.0 ± 20.0	211.0	203.0
	$E = 1200$ MeV, $\sigma_R = 1719$ mb		
0–2 MeV		6.0	7.0
2–20 MeV	52.0 ± 6.0	54.0	78.0
20–E_{beam}	318.0 ± 30.0	309.0	294.0
	$E = 1600$ MeV, $\sigma_R = 1717$ mb		
0–2 MeV		6.0	8.0
2–20 MeV	65.0 ± 8.0	61.0	97.0
20–E_{beam}	410.0 ± 40.0	422.0	373.0

are consistent, within error bars, with both models. Looking at Table II, it can be noticed that most of the ejected energy is taken away by cascade neutrons. The experimental average carried energies are always closer to the Cugnon than to the Bertini INC values. This suggests that the energy balance is more realistic in the Cugnon model, in which more energy is taken away by cascade particles and less excitation energy is left at the end of the INC stage. This could be mostly ascribed to the fact that the Pauli blocking is handled in a more subtle way by Cugnon, as discussed in [21], than by Bertini in which too many high energy collisions are blocked. In conclusion, the replacement of the Bertini by the Cugnon INC model, in the TIERCE code, leads to a significantly better agreement with our experimental data, the improvements coming mainly from the more realistic description of the *NN* cross sections and treatment of the Pauli blocking.

We thank O. Bersillon, J. Cugnon, H. Duarte, and C. Volant for helping us with the code calculations.

[1] G. S. Bauer, in *Proceedings of the 2nd International Conference on Accelerator Driven Transmutation Technologies, Kalmar, Sweden, 1996,* edited by H. Condé (Uppsala University, Uppsala, 1996), p. 159.
[2] Review of the Spallation Neutron Source (SNS), Department of Energy Report No. DOE/ER-0705, 1997.
[3] J. M. Carpenter, Nucl. Instrum. Methods **145**, 91 (1977).
[4] J. C. Browne *et al.,* in *Proceedings of the 2nd International Conference on Accelerator Driven Transmutation Technologies, Kalmar, Sweden* (Ref. [1]), p. 101.
[5] J. L. Flament, in *Proceedings of the 2nd International Workshop on Spallation Materials Technology, Ancona, Italy, 1997,* edited by F. Carsughi, L. K. Mansur, W. F. Sommer, and H. Ullmeier (KFA Jülich, Jülich, 1997), p. 71.
[6] C. D. Bowman *et al.,* Nucl. Instrum. Methods Phys. Res., Sect. A **320**, 336 (1992).
[7] T. Takizuka, in *Proceedings of the International Conference on Accelerator-Driven Transmutation Technologies and Applications, Las Vegas, 1994,* edited by E. D. Arthur, A. Rodriguez, and S. O. Schriber (AIP Press, Woodbury, NY, 1995), p. 64.
[8] C. Rubbia *et al.,* Report No. CERN/AT/95-44(ET), 1995.
[9] M. Blann *et al., International Code Comparison for Intermediate Energy Nuclear Data* (OECD/NEA, Paris, 1994).
[10] F. Borne *et al.,* Nucl. Instrum. Methods Phys. Res., Sect. A **385**, 339 (1997).
[11] E. Martinez *et al.,* Nucl. Instrum. Methods Phys. Res., Sect. A **385**, 345 (1997).
[12] S. Leray *et al.,* in *Nuclear Data for Science and Technology,* Conference Proceedings Vol. 59, edited by G. Reffo, A. Ventura, and C. Grandi (SIF, Bologna, 1997), p. 1426.
[13] I. Tilquin *et al.,* Nucl. Instrum. Methods Phys. Res., Sect. A **365**, 446 (1995).
[14] J. Thun *et al.* (to be published).
[15] R. A. Arndt *et al.,* Phys. Rev. C **50**, 2731 (1994).
[16] B. E. Bonner *et al.,* Phys. Rev. C **18**, 1418 (1978).
[17] W. B. Amian *et al.,* Nucl. Sci. Eng. **112**, 78 (1992).
[18] T. Nakamoto *et al.,* J. Nucl. Sci. Tech. **32-9**, 827 (1992).
[19] O. Bersillon, in *Proceedings of the 2nd International Conference on Accelerator Driven Transmutation Technologies, Kalmar, Sweden* (Ref. [1]), p. 520.
[20] H. W. Bertini *et al.,* Phys. Rev. **131**, 1801 (1963).
[21] J. Cugnon, C. Volant, and S. Vuillier, Nucl. Phys. **A620**, 475 (1997).
[22] T. W. Armstrong and K. C. Chandler, Nucl. Sci. Eng. **49**, 110 (1972).
[23] Los Alamos National Laboratory Report No. LA-12625, 1993, edited by J. F. Briesmeister.
[24] L. W. Dresner, Oak Ridge Report No. ORNL-TM-196, 1962.
[25] J. Cugnon, Nucl. Phys. **A462**, 751 (1987).
[26] J. Cugnon *et al.,* Phys. Rev. C **56**, 2431 (1997).
[27] B. C. Barashenkov, *Cross Sections of Interactions of Particle and Nuclei with Nuclei* (JINR, Dubna, 1993).